Journal of Power Sources 229 (2013) 265–271

Contents lists available at SciVerse ScienceDirect

Journal of Power Sources

journal homepage: www.elsevier.com/locate/jpowsour

# Intercalation and conversion reactions in $Ni_{0.5}TiOPO_4$ Li-ion battery anode materials

Karima Lasri [a], Mohammed Dahbi [b], Anti Liivat [b], Daniel Brandell [b], Kristina Edström [b], Ismael Saadoune [a,*]

[a] LCME, FST Marrakech, University Cadi Ayyad, BP549, Av. A. Khattabi, Marrakech 40000, Morocco
[b] Department of Chemistry – Ångström, ALISTORE-ERI, Uppsala University, PO Box 538, SE-751 21 Uppsala, Sweden

## HIGHLIGHTS

- $Ni_{0.5}TiOPO_4$ anode material was synthesized by sol–gel method directly from $H_3PO_4$ acid.
- The small particle size and the carbon coating of $Ni_{0.5}TiOPO_4$ lead to enhanced electrochemical performance.
- *Ex-situ* XRD analysis during the first discharge shows an amorphization of this anode material.
- A model explaining the anomalous 1st discharge capacity and the amorphization of this phosphate was proposed.

## ARTICLE INFO

*Article history:*
Received 18 October 2012
Received in revised form
28 November 2012
Accepted 6 December 2012
Available online 13 December 2012

*Keywords:*
Li-ion batteries
Anode materials
$Ni_{0.5}TiOPO_4$
Sol–gel
Conversion reaction

## ABSTRACT

The $Ni_{0.5}TiOPO_4$/C composite Li-ion battery anode material has been prepared by a sol–gel method with a subsequent pyrolysis step for the formation of C-coating. The resulting sub-micronsized particles displayed a narrow particle size distribution and a corresponding high electrochemical activity which, in turn, facilitates in-depth analysis of the electrochemical behavior of the material. It is shown that by limiting the degree of lithiation in the material, the redox potential in subsequent cycles is substantially affected. *Ex-situ* XRD reveals a gradual evolution of the structure during cycling of the material, with lower crystallinity after the first discharge cycle. By correlating the electrochemical properties with the structural studies, new insights into the electrochemical behavior of the $Ni_{0.5}TiOPO_4$/C anode material are achieved, suggesting a combination of intercalation and conversion reactions.



## 1. Introduction

Currently, graphite and other carbon materials are used as anodes for commercial lithium-ion batteries. However, safety concerns regarding graphite anodes have led to a search for alternative anode materials. One strategy to reach safety is using anodes based on titanium compounds, which operate at potentials typically above the threshold of reductive decomposition of conventional electrolytes. These materials, however, experience shortcomings due to the limited amount of charge that can be reversibly stored in them. In this respect, complexes of Transition Metal (TM) oxides with Ti-compounds seem to be promising to achieve a complete utilization of the redox-capable species in the material, as has recently been demonstrated for nickel titanium oxyphosphates [1–5].

Preparation and structural characterisation of $Ni_{0.5}TiOPO_4$ was firstly described in 1998 [6]. The monoclinic structure of $Ni_{0.5}TiOPO_4$ is built up of a corner-sharing framework consisting of chains of $TiO_6$ octahedra which are linked by $PO_4$ tetrahedra. This framework structure belongs to a family of closely related structures known as tavorites, sillimanites and triplites, which has recently attracted much attention for use as cathode materials for both Li- and Na-batteries [7]. In this structure, Ni-ions occupy octahedrally coordinated sites sharing faces with the $TiO_6$ octahedra. Such crystal structure also provides three-dimensionally connected empty sites for intercalation of guest ions with various sizes, including lithium ions. Lithium insertion into $Ni_{0.5}TiOPO_4$ results in a reduction of $Ti^{4+}$ at the octahedral site 4(e) and of $Ni^{2+}$ located at octahedral site 2(a) sites. More than two lithium ions can be inserted with a reversible specific capacity above 200 mAh $g^{-1}$ [1–5].

The main challenge of the micronsized $Ni_{0.5}TiOPO_4$ material made initially was its low electronic conductivity and a large

* Corresponding author. Tel.: +212 6 61 48 64 64; fax: +212 5 24 43 31 70.
*E-mail addresses:* i.saadoune@uca.ma, saadoune1@yahoo.fr (I. Saadoune).

0378-7753/$ – see front matter © 2012 Elsevier B.V. All rights reserved.
http://dx.doi.org/10.1016/j.jpowsour.2012.12.031

irreversible capacity [1]. After carbon coating the surface of the material particles, the stability of electrode material and its recycling performance have been substantially improved [2–5]. Nevertheless, much of the underlying redox processes remain poorly resolved. In particular, the first cycle redox process is different from the subsequent cycles and remains puzzling, especially considering some variation in the data in earlier reports [1–3]. One reason for this variation in the electrochemical properties could well be the influence of the preparation method – the properties of the particles depend significantly on the synthesis process, which lead to final products with a range of sizes and morphologies. Furthermore, although the theoretical capacity of $Ni_{0.5}TiOPO_4$ is equal to 285 mAh $g^{-1}$, if corresponding to the insertion of 1.5 $Li^+$ ions and reduction of both $Ni^{2+}$ and $Ti^{4+}$ ions, most of the reported results on this system have revealed anomalous first discharge capacity (>350 mAh $g^{-1}$). Nevertheless, the origin of this large discharge capacity remains unclear.

In this paper, we report on the preparation and functionality of highly electrochemically active $Ni_{0.5}TiOPO_4$/C composites, resulting from a sol–gel process which allows a high degree of mixing of the reactants. Furthermore, the small particle size and narrow particle size distribution also allow observations of a more detailed picture of the involved redox processes than what has been previously reported. A model explaining the 1st discharge process of Li//$Li_x$-$Ni_{0.5}TiOPO_4$/C batteries is also proposed and discussed.

## 2. Experimental

$Ni_{0.5}TiOPO_4$ was prepared using a sol–gel method. A mixed solution of $H_3PO_4$ (98%, Fluka) and $TiCl_4$ diluted in ethanol (98%, Prolabo) was added drop-wise onto a $Ni(NO_3)_2.6H_2O$ (97%, Prolabo) powder under magnetic stirring for one hour. An adequate water volume was added to maintain a pH equal to 0 in which the gel was formed. The gel was dried at 100 °C for 5 h to remove excess ethanol, thereafter heated at 550 °C for 5 h in air and finally calcined at 650, 750, 850 and 950 °C sequentially for 18 h with intermediate grinding for 1 h.

A $Ni_{0.5}TiOPO_4$/C composite was synthesized from the green $Ni_{0.5}TiOPO_4$ powders and sucrose. Amounts of sucrose (15 wt.%) and $Ni_{0.5}TiOPO_4$ (85 wt.%) were mixed with acetone. Thermal treatment under flowing Argon gas was performed at 600 °C for 5 h where after a black powder indentified as a carbon-coated $Ni_{0.5}TiOPO_4$ composite was obtained.

The phase identification of the synthesized products was carried out by X-ray diffraction (XRD; Siemens D5000 diffractometer) using Cu Kα radiation (λ = 1.5418 Å). Lattice parameters of $Ni_{0.5}TiOPO_4$/C were refined using Rietveld methodology implemented by the Fullprof program [6]. The morphology of the sample was observed by high resolution scanning electron microscopy (SEM; HRSEM LEO 1550). The specific surface area of the prepared samples was evaluated by $N_2$ gas adsorption and desorption measurements (Micrometrics ASAP 2020 Accelerated Surface Area and Porosimetry Analyzer) using a Brunauer–Emmett–Teller (BET) method; the samples were dried for 10 h at 300 °C under nitrogen gas before measurement. A Q500 Thermogravimetric Analyzer was used for thermogravimetric analysis (TGA) using a heating rate of 15 °C $min^{-1}$ from 50 to 600 °C in air atmosphere. The Raman shift spectra of the samples were achieved using a Renishaw 2000 Raman spectrometer with a scanning range of 100–2000 $cm^{-1}$.

$Ni_{0.5}TiOPO_4$ electrodes were fabricated by mixing a 75:15:10 (w/w) ratio of active material, a carbon (Super P) electronic conductor and polyvinylidene fluoride (PVDF) binder, using *N*-methyl-2-pyrrolidine (NMP) as solvent. The mixture was thereafter pasted on a Cu foil. After drying overnight at 60 °C, the electrodes were cut into circular shapes for cell assembly.

Lithium was used as counter electrode, and 1 M $LiPF_6$ in ethylene carbonate and diethyl carbonate (EC:DEC = 2:1 by volume) was used as electrolyte. All cells were assembled in an Ar glove box, and the electrochemical tests were carried out at room temperature.

The cells were cycled galvanostatically at different current rates using a Digatron BTS 600 battery tester. Further details on the redox processes and their kinetics were obtained using Galvanostatic Intermittent Titration Technique (GITT) and cyclic voltammetry (CV) carried out on a VMP cycling system. GITT data was collected in 1 h pulses of ~10 mA $g^{-1}$ (C/20 rate) followed by 1 h relaxation time; CV data were collected at scan rates 0.01 mV $s^{-1}$ and 0.1 mV $s^{-1}$.

Electrodes from cells lithiated to a degree of i) $x = 0.5$, ii) 1.0, iii) 2.0, iv) >3.0 in $Li_xNi_{0.5}TiOPO_4$ and v) after a full lithiathion–delithiation cycle have been disassembled in an Ar glove box, washed in Dimethyl Carbonate (DMC) where after *ex-situ* diffraction patterns have been recorded at the MAXLab synchrotron facility.

## 3. Results and discussion

### 3.1. Materials characterization

XRD patterns of the $Ni_{0.5}TiOPO_4$ powders are shown in Fig. 1a. The diffraction peaks can be indexed on the monoclinic $Ni_{0.5}TiOPO_4$

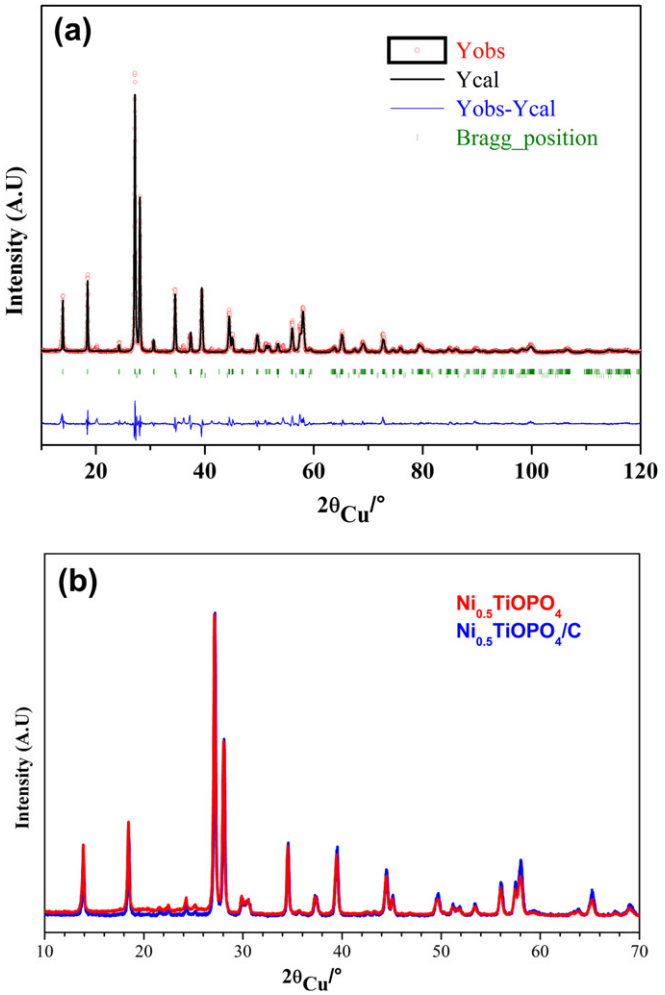


**Fig. 1.** (a) Rietveld refinement results of X-ray diffraction pattern of $Ni_{0.5}TiOPO_4$ powder. (b) XRD patterns of the $Ni_{0.5}TiOPO_4$ and $Ni_{0.5}TiOPO_4$/C materials.

structure with the space group $P2_1/c$ [8] as the main phase with a few low-intensity peaks mainly attributed to $TiO_2$ rutile. Indeed, Rietveld refinement with the hypothesis of $TiO_2$–$Ni_{0.5}TiOPO_4$ mixture evidenced that the quantity of $TiO_2$ is less than 1%. The peak around 20° could be attributed to $Ni_2P_2O_7$ (JCPDS#75-1054). In the $Ni_{0.5}TiOPO_4$/C composite diffractogram (Fig. 1b), only peaks of monoclinic $Ni_{0.5}TiOPO_4$ can be observed, indicating that the carbon in the composite is amorphous and that the phase remained pure under the formation of the C-coating.

Fig. 2 shows the Raman spectra of $Ni_{0.5}TiOPO_4$ and the $Ni_{0.5}TiOPO_4$/C composites. The sharp band at 750 $cm^{-1}$ in Fig. 2a is attributed to the vibration of the –Ti–O–Ti–O–chains, while the bending and stretching vibrations of the $PO_4^{3-}$ -group are found in 390–630 $cm^{-1}$ and 860–1130 $cm^{-1}$ regions, respectively. The signals located in the low wavenumber region correspond to translational vibrations of the $Ti^{4+}$, $Ni^{2+}$ and $PO_4^{3-}$ ions and $PO_4^{3-}$ librations [6]. Furthermore, the broad bands in Fig. 2b are characteristic of carbon and suggest coatings of structurally ordered carbon on $Ni_{0.5}TiOPO_4$. The strong band at 1596 $cm^{-1}$ in Fig. 2b, which is usually referred to as the graphite band (G-band), is characteristic of carbon materials with a high degree of structural order [9,10]. This band corresponds to one of the modes arising from the movement in opposite directions of the two neighboring carbon atoms in a graphene sheet. The band observed at 1354 $cm^{-1}$ in Fig. 2b, called the disorder-induced phonon mode (D-band), corresponds to the vibrations at the edges of graphene sheets [11].

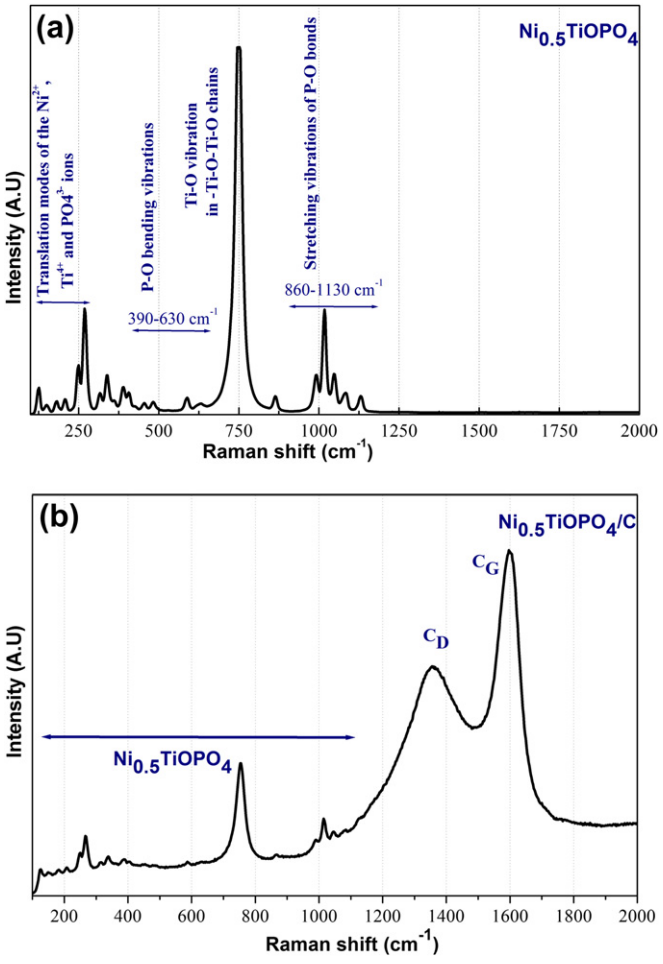


**Fig. 2.** Raman spectra for $Ni_{0.5}TiOPO_4$ (a) and $Ni_{0.5}TiOPO_4$/C (b) with predominant bands marked.

The $I_D/I_G$ value (the peak intensity ratio between the 1354 and 1596 $cm^{-1}$ peaks) generally provides a useful index for comparing the degree of crystallinity of predominately $sp^2$-type carbon materials, i.e., the smaller the ratio of $I_D/I_G$, the higher the degree of ordering in the carbon material. The $I_D/I_G$ ratio ($I_D/I_G$ = 0.67) in Fig. 2b indicates predominately planar graphitic ordering in the carbon coated on $Ni_{0.5}TiOPO_4$ [12], which should support the electronic distribution over the active material, yet allowing Li transport through it.

To estimate the amount of carbon present in the $Ni_{0.5}TiOPO_4$/C composite and determine the changes in sample weight with increased temperature, TGA analysis was carried out from 50 to 600 °C in air. Fig. 3 shows the TGA curves of $Ni_{0.5}TiOPO_4$ and $Ni_{0.5}TiOPO_4$/C. The composite powders start to lose weight slowly at a temperature of approximately 150 °C, while the $Ni_{0.5}TiOPO_4$ powders remain stable over the whole temperature range. Therefore, the amount of amorphous carbon in the $Ni_{0.5}TiOPO_4$/C composite can be estimated to be approximately 3 wt.%.

The morphology of the $Ni_{0.5}TiOPO_4$/C composite is shown in Fig. 4, where submicrometer-sized particles with agglomeration are clearly visible. Brunauer–Emmett–Teller (BET) nitrogen-adsorption measurements show that the specific surface area of the $Ni_{0.5}TiOPO_4$/C composite is 28.48 $m^2\ g^{-1}$ clearly indicating submicron-sized particles. For such a particle morphology, 3 wt.% of carbon is typically sufficient to substantially improve the electronic wiring and thereby the electrochemical activity of the material [12].

### 3.2. Electrochemical measurements

#### 3.2.1. Cycling performance

Galvanostatic charge and discharge measurements were carried out for $Ni_{0.5}TiOPO_4$/C composites. Fig. 5 shows the first charge–discharge curves for the $Ni_{0.5}TiOPO_4$/C electrode, measured between 0.5 and 3 V at C/20 rate. The first discharge curve shows two quasi-plateaus at ~1.4 V and ~1.1 V before the onset of the SEI-formation region, a phenomenon recently reported [4,5]. This is different from other studies [1–3], which show only a single plateau near 1.2 V. Such differences in electrochemical behavior could not be attributed to the structure of the materials, since the X-ray diffraction data is similar. In our work, the sol–gel method gives a large specific surface area (28.48 $m^2\ g^{-1}$) and a small average particle size (200–100 nm), which should increase the electrochemical reactivity through rapid lithium-ion diffusion and thereby also enhancing the capacity retention even at high rates

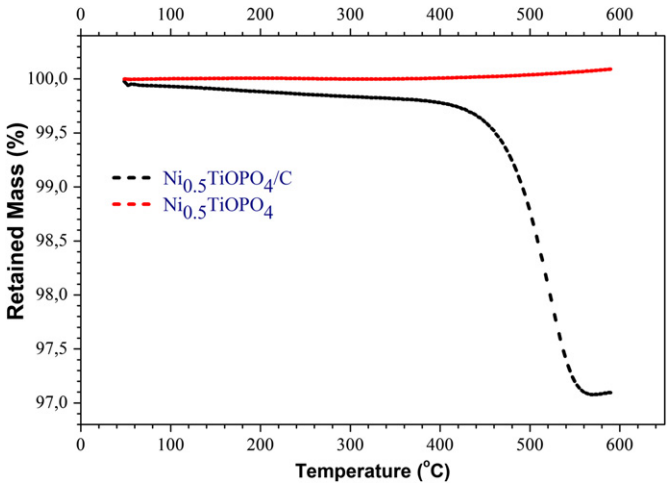


**Fig. 3.** TGA curves of $Ni_{0.5}TiOPO_4$ and $Ni_{0.5}TiOPO_4$/C composite.

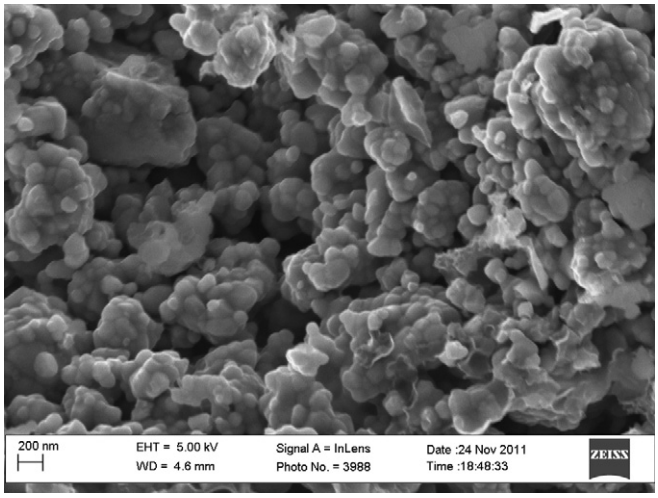


**Fig. 4.** SEM image of the $Ni_{0.5}TiOPO_4$/C composite.

[13]. It is therefore more likely that morphological effects have a major influence not only on the electrochemical performance but also by separating different redox processes, as seen during the first discharge of the $Ni_{0.5}TiOPO_4$/C material.

The inset in Fig. 5 shows that there is a higher polarization, ~0.5 V, in the beginning of the lithiation which, however, decreases significantly at the later stage of insertion. Such a decrease of polarization during the first delithiation is also consistent with earlier impedance measurements [1] of uncoated samples. This aspect suggests that the improvement of lithiation kinetics during the first discharge also involves a change in the electronic properties of the composite. Such an improvement in electrode kinetics could well be expected if a complementary electronically conductive material is formed through the reduction of $Ni^{2+}$ to metallic Ni; i.e., through a conversion reaction.

The first discharge capacity of the $Ni_{0.5}TiOPO_4$/C electrode is 488 mAh $g^{-1}$, which is much higher than the theoretical capacity of the material (285 mAh $g^{-1}$), estimated from the redox pairs $Ti^{4+}$/$Ti^{3+}$ and $Ni^{2+}$/$Ni^0$. This extra capacity seems to originate in the growth of a solid electrolyte interface (SEI) layer on the surface of the particles during the first discharge. About half of this extra discharge capacity is obtained above the typical onset potential (~0.8 V) for carbonate-based electrolyte decomposition reactions on lithium metal or graphitic anodes. The high reactivity seen here resembles that of conversion reactions of TM-oxides, which lead to the formation of very fine TM nanoparticles able to substantially enhance the electrolyte decomposition reactions [14].

The first charge process exhibits a higher voltage plateau than the discharge processes, with a sloping potential near 1.6 V, and is reversible in the following cycles. Fig. 6 displays the discharge capacity *vs.* cycle number for different rates: C/20, C/10, C/5 and C. After 18 cycles, the obtained discharge capacity was 268, 250, 235 and 224 mAh $g^{-1}$, respectively. After rapid cycling at C-rate, the battery recovered a capacity of 242 mAh $g^{-1}$ at C/5-rate (Fig. 7) which is excellent recovery.

In Table 1, the low-rate electrochemical properties of our $Ni_{0.5}TiOPO_4$/C material are compared to other $Ni_{0.5}TiOPO_4$/C composites reported in literature. From the comparison, a positive correlation between the first discharge capacity and the smaller particle size obtained by the sol–gel process can be seen – the material synthesized here is clearly among the ones displaying higher capacity. At the same time, the irreversible capacity loss in the range of 40–50% still seems to be present. The other material displaying comparatively high capacity after similar cycling was synthesized using precipitation methods [3]; however, this strategy resulted in an inhomogeneous particle size distribution which does not enable in-depth studies of the electrochemical behavior of the material. This was also the conclusion when studying the electrochemical behavior of the $Ni_{0.5}TiOPO_4$ material depending on particle size [5].

### 3.2.2. *Structural evolution during cycling*

Preliminary *in-situ* diffraction studies revealed a tendency for a decrease in crystallinity of $Li_xNi_{0.5}TiOPO_4$/C with increasing *x*. Due to peak overlap of the active material with the strong background from packaging, *ex-situ* XRD investigations of pre-cycled batteries to a pre-defined state were carried out. The diffraction patterns of $Ni_{0.5}TiOPO_4$ cells discharged from 3 V to 0.5 V and charged from 0.5 V to 3 V are shown in Fig. 8. The XRD patterns indeed illustrate how the crystallinity of $Ni_{0.5}TiOPO_4$/C disappears after insertion of

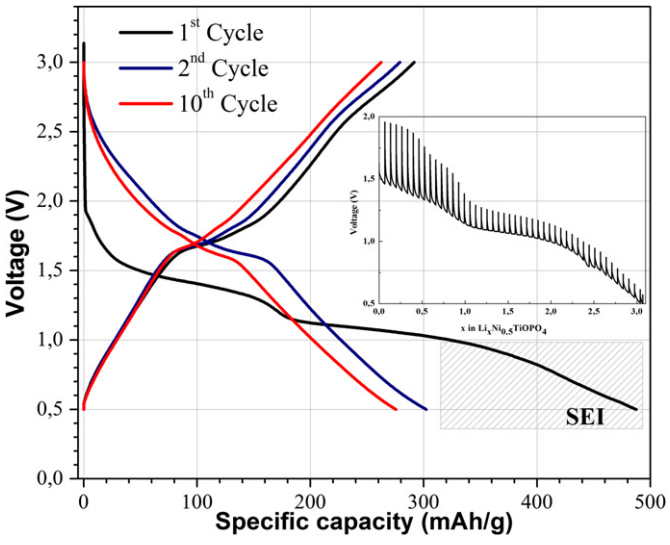


**Fig. 5.** The 1st, 2nd and 10th charge and discharge curves for $Ni_{0.5}TiOPO_4$/C, cycled at C/20 rate (20 h discharge or charge time) from 0.5 to 3.0 V; the highlighted area shows capacity originating from reactions at the electrode–electrolyte interface. The inset shows the evolution of potential with respect to *x* in $Li_xNi_{0.5}TiOPO_4$ during first discharge from GITT.

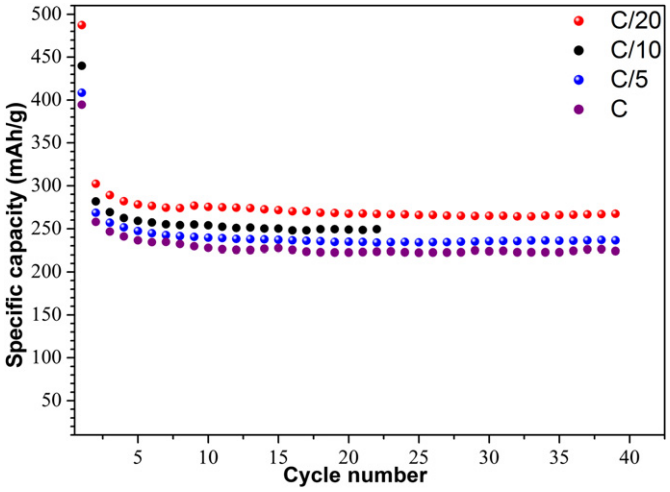


**Fig. 6.** The discharge capacities for Li||$Ni_{0.5}TiOPO_4$/C cells cycled from 0.5 to 3.0 V at different C-rates for 18 cycles.

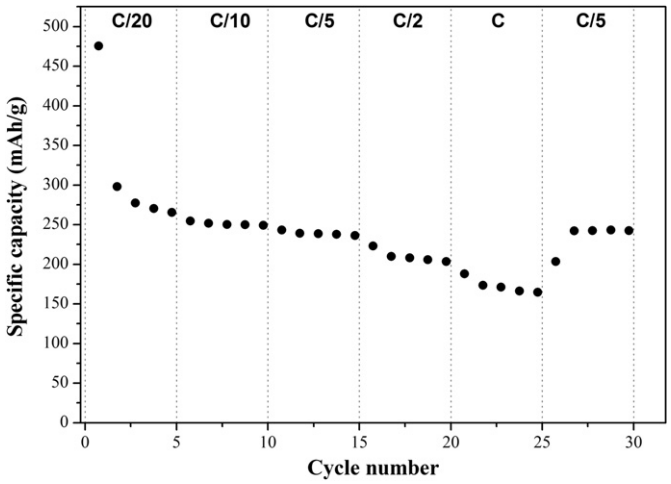


**Fig. 7.** The rate performance of Li||$Ni_{0.5}TiOPO_4$/C cells cycled from 0.5 to 3.0 V.

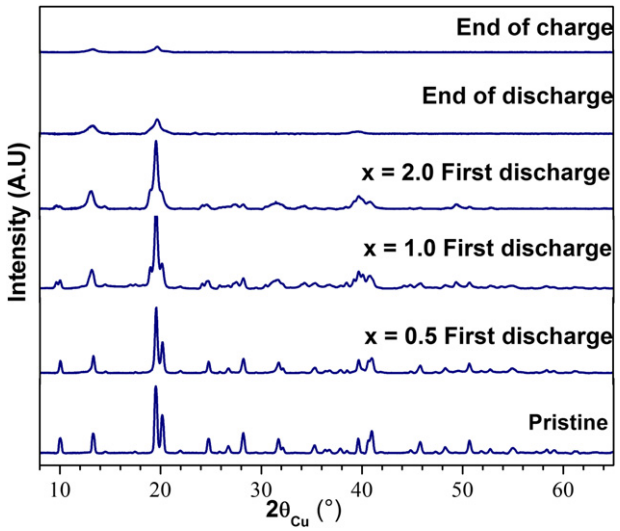


**Fig. 8.** *Ex-situ* XRD patterns of the $Li_xNi_{0.5}TiOPO_4$.

two lithium ions. If compared to the pristine sample, the most noticeable differences appear after the insertion of the first lithium ion per formula unit, where new peaks emerge and the initial peaks have broadened substantially. It is remarkable that despite the more complex redox behavior of the $Ni_{0.5}TiOPO_4$/C samples presented here (discussed below), the overall picture of the lithiation-induced changes in the diffraction pattern closely follow that reported in an earlier synchrotron study [4].

From structural point of view, there are only three available octahedral positions for lithium ions during the lithiation process, corresponding to the 2b, 2c and 2d sites in $P2_1/c$ space group. Each of these sites could accommodate 0.5 $Li^+$ ion/formula unit. Therefore, theoretically only 1.5 lithium ions can be inserted in $Ni_{0.5}TiOPO_4$. Nevertheless, when all these positions are filled by lithium, a strong repulsion between the cations follows as a result of the short atomic distances between these crystallographic positions. Structurally unstable $Li_xNi_{0.5}TiOPO_4$ phases were thus formed during the lithiation, leading to a phase separation and/or amorphization of the electrode material. This behavior has been reported from Mössbauer spectroscopy studies of the lithiation process in the homologous phase of $Fe_{0.5}TiOPO_4$ [15]. In this case, lithium insertion induces an amorphization of the electrode material and the appearance of Fe metal.

In short, the lithiation process involves an initial step of topotactic lithiation of the pristine structure ($x < 0.5$), followed by a growth of a new crystalline phase in parallel to a gradual amorphisation of both structures. It is also remarkable that the lithiation of the Ni-free counterpart $LiTiOPO_4$ led to a similar decrease of crystallinity [16]. This implies that the loss of spatial correlation probed by XRD for this family of compounds is not caused only by the presence of electrochemically active Ni-ions in the lattice.

**Table 1**
Comparison of the electrochemical properties of $Ni_{0.5}TiOPO_4$/C powders synthesized in this work with data reported in literature.

| Samples | Cycling rate | Potential range (V) | Initial specific capacity (mAh $g^{-1}$) | Capacity retention (mAh $g^{-1}$) | Ref. |
|---|---|---|---|---|---|
| $Ni_{0.5}TiOPO_4$/C | C/20 | 0.5–3.0 | 488 | 265 after 30 cycles | This work |
| $Ni_{0.5}TiOPO_4$ | C/15 | 0.5–4.0 | 415 | 200 after 20 cycles | [1] |
| $Ni_{0.5}TiOPO_4$/C[a] | C/20 | 0.9–3.0 | 352 | ≈195 after 30 cycles | [2] |
| $Ni_{0.5}TiOPO_4$/C | ≈C/13 | 0.5–3.0 | 530 | 276 after 30 cycles | [3] |
| $Ni_{0.5}TiOPO_4$/C | ≈C/13 | 0.5–3.0 | 530 | – | [4] |
| $Ni_{0.5}TiOPO_4$ | ≈C/13 | 0.5–3.2 | ≈500 | – | [5] |

[a] Carbon coating formed at low temperature (300 °C).

### 3.2.3. Cyclic voltammetry

*3.2.3.1. Low potential cut-off.* Galvanostatic cycling between 0.5 and 3 V confirmed that the synthesized $Ni_{0.5}TiOPO_4$/C composite suffers from a significant capacity loss between the first and second cycle, similar to previous studies [1–3], and most probably primarily associated with SEI layer formation. In order to get a more detailed picture of the involved redox processes, cyclic voltammetry (CV) has been carried out, first between 3 and 0.5 V. A rather complex redox activity can be witnessed from the CV curves of $Ni_{0.5}TiOPO_4$/C electrode (see Fig. 9). In the first anodic scan, the reduction starts with a small peak at 1.90 V, after which the current continues to increase as the potential is lowered further. Two obvious peaks emerge: one at ~1.25 V followed by a stronger at ~0.98 V. The activity at higher voltage values, from 1.9 V across the

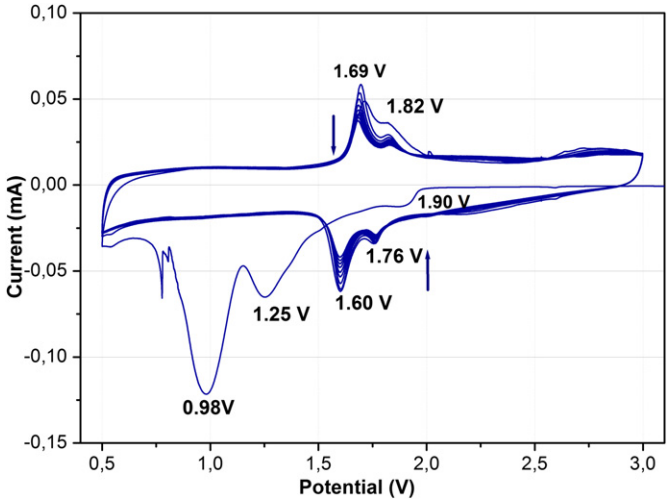


**Fig. 9.** Cyclic voltammograms of $Ni_{0.5}TiOPO_4$/Celectrodes measured between 0.5 and 3.0 V at a scan rate of 0.01 mV $s^{-1}$. The arrows indicate changes during cycling.

first peak at 1.25 V, corresponds to the $Ti^{4+}/Ti^{3+}$ or $Ni^{2+}/Ni^{0}$ reduction. The second reduction peak at 0.98 V is the main contribution of irreversible capacity loss in the first cycle. However, after the first cycle, the original reduction peaks disappear and a new doublet – related either to the separation of the activity of the redox pairs or to different structures in the material – at 1.60 V and 1.76 V appears instead.

In the first subsequent oxidation process, a substantial amount of charge is transferred under a quasi-constant current profile on top of which are two peaks at 1.69 V and ~1.82 V. These peaks may be attributed to the oxidation of $Ti^{3+}$ back to $Ti^{4+}$ and $Ni^{0}$ to $Ni^{2+}$ in the more ordered remnants of the lithiated phase, whereas the quasi-constant current originates either from a single-phase insertion process or from a large non-faradaic (capacitive) contribution.

The shape of the CV curve in the following cycles remained similar to that in the second cycle, with a good reversibility but somewhat further decrease of the peak intensity in the range 1.7–1.8 V could be observed. Despite substantial changes in the material structure after the first cycle, the stable capacity in the subsequent cycles implies that a good passivation of the composite electrode has been achieved during the first cycle(s).

*3.2.3.2. High potential cut-off.* In order to achieve a more detailed picture of the reversible redox processes, cyclic voltammetry was carried out at 0.01 mV $s^{-1}$ from 1.1 to 3.2 V, thereby excluding the intense anodic reaction at 0.98 V of possible SEI-origin. During the first reduction sweep (Fig. 10) one anodic peak at 1.25 V is observed, similar to the one seen when using a low potential cut-off. In contrast, a new strong anodic peak at high (1.94 V) potential is seen in the subsequent cycles. Interestingly, the intensity of this peak gradually decreases whereas the doublet in the 1.6–1.8 V potential range – also seen with low cut-off (Fig. 9) – emerges (Fig. 10). During the first cathodic process, a new peak at 2.12 V is present, clearly matching the anodic peak at 1.94 V. The relatively low-intensity peak at 1.68 V, on the other hand, seems to match the anodic activity in the 1.6–1.8 V range.

In the six subsequent cycles (Fig. 10), the initially intense anodic and cathodic peaks at 1.94 V and 2.12 V, respectively, disappear. At the same time, two small cathodic peaks at 1.715 V and 1.81 V, corresponding to the anodic peaks at 1.60 and 1.75 V, grow in intensity to the extent that the CV becomes very similar to the CV recorded using low potential cut-off. Despite this similarity, the capacity originating from the flat, non-faradaic current profile for high potential cut-off is much lower than that of the material cycled to lower cut-off voltage, as judged by the peak areas in the CV curves.

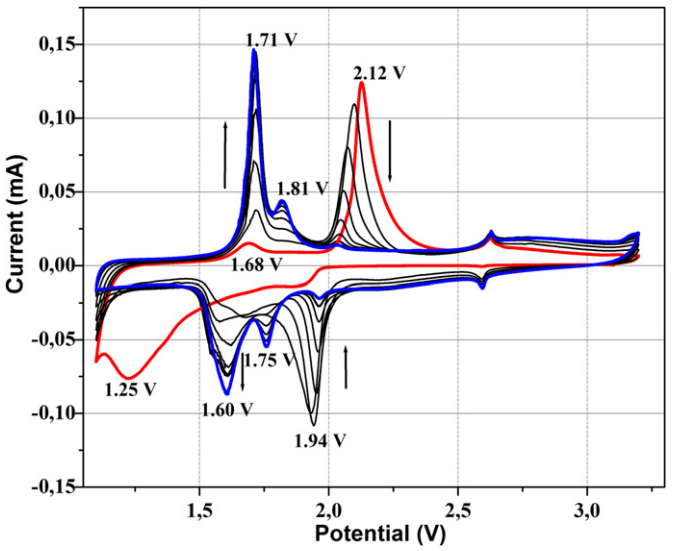


**Fig. 10.** Cyclic voltammograms of $Ni_{0.5}TiOPO_4/C$ electrodes recorded between 1.1 and 3.0 V at a scan rate of 0.01 mv $s^{-1}$ shown in different color, 1st cycle in red, 8th in blue and cycles 1–7 in black. The arrows indicate changes during cycling. (For interpretation of the references to colour in this figure legend, the reader is referred to the web version of this article.)

*3.2.3.3. Discussion.* As stated above, the CV data indicates both insertion and conversion mechanisms in the $Ni_{0.5}TiOPO_4$ compound. Regarding the insertion, which occurs at potentials above 1.25 V, a comparison with the structurally related compounds $Ti_{0.25}TiOPO_4$ [17] and $LiTiOPO_4$ [16] can be useful. The first structure, which has more vacant sites in the lattice, exhibits redox activity mostly at higher potentials, ~2 V. $LiTiOPO_4$, on the other hand, experience Li-insertion predominately at lower potentials, ~1.5 V. $Ni_{0.5}TiOPO_4$ falls in between these two materials where the insertion of up to 0.5 Li/fu takes place at potentials higher than 1.5 V (Fig. 5). A high cut-off for the reduction potential apparently inhibits a too excessive lithiation and a corresponding structural reorganization, and could be one reason why the high-voltage redox activity near 2 V persists over several CV cycles.

The conversion mechanism related to $Ni^{2+}/Ni^{0}$ transitions, appearing at lower potentials, deserves special attention since the reversibility of this process is crucial for maintaining a large reversible capacity of this compound. The main aspects of the conversion reactions are well known from the lithiation of transition metal oxides MO (M = Ni, Co, Fe, Cu...) [18]. The electrochemical reduction of these oxides leads to a formation of a mixture of $Li_2O$ and metallic M nanoparticles. Such a morphological rearrangement leads to an enhancement of the electrode/electrolyte reactions, thereby explaining the large irreversible capacity observed in these conversion materials during the first cycle. However, it is difficult to relate the redox processes observed here to the two cathodic/anodic conversion peaks at 1.22 V and 2.2 V, respectively, found for NiO anodes [19,20]. First, it would be inconsistent with the suggestion that the high-voltage peaks originate from an insertion process. Second, unlike NiO, these peaks are not visible in subsequent cycles. It is more likely that the $Ni/Ni^{2+}$ redox couple in $Ni_{0.5}TiOPO_4$ is active over a broader potential window as compared to that of NiO. In particular, the presence of an oxyphosphate framework may strongly influence the nucleation and the morphology of Ni during the first discharge. This is not surprising considering that the equilibrium potential for the reaction $NiO + 2Li^+ + 2e^- \rightarrow Ni + Li_2O$ is ca. 1.8 V [21] (i.e., different from the two main redox peaks at 1.22 and 2.2 V), and substantial intrinsic kinetics and confinement effects thus strongly influence the measured $Ni/Ni^{2+}$ potential.

## 4. Conclusions

Nickel titanium oxyphosphate $Ni_{0.5}TiOPO_4/C$ anode material was successfully prepared by a sol–gel method, resulting in a small particle size with a narrow enough particle size distribution to offer good electrochemical reactivity for in-depth analysis of the redox processes. The electrochemical testing demonstrates that the short lithium diffusion path length in the synthesized $Ni_{0.5}TiOPO_4/C$ sample leads to good electrochemical properties, seen as high rate capability and good cycle stability. There is an obvious difference in the electrochemistry between the first and the following cycles: a high capacity is delivered during the first cycle, which can be contributed to a conversion reaction during the first discharge. The CV data show that an interplay exist between intercalation and conversion reactions which depend substantially on the degree of

lithiation. Moreover, results from *ex-situ* XRD studies on the $Ni_{0.5}TiOPO_4$/C electrodes suggest that the material undergoes an amorphisation after insertion of two Li/fu. The electrochemical properties of $Ni_{0.5}TiOPO_4$/C are obviously dependent on the crystallinity, morphology and particle size. Optimization of the microstructure can indeed improve the electrochemical performance, but has not yet succeeded to reduce the large irreversible capacity loss during the first cycle.

## Acknowledgements

A scholarship from the J Gust. Richert Foundation is greatly acknowledged. Thanks to CNRST, Morocco, for the financial support under the RS program (RS03/2011).

## References

[1] I. Belharouak, K. Amine, Electrochem. Commun. 7 (2005) 648–651.
[2] K. Maher, K. Edström, I. Saadoune, T. Gustafsson, M. Mansori, J. Power Sources 196 (2011) 2819–2825.
[3] X.J. Zhang, Y. Zhang, Z. Zhou, J.P. Wei, R. Essehli, B. El Bali, Electrochim. Acta 56 (2011) 2290–2294.
[4] R. Essehli, B. El Bali, A. Faik, S. Benmokhtar, B. Manoun, Y. Zhang, X.J. Zhang, Z. Zhou, H. Fuess, J. Alloys Compd. 530 (2012) 178–185.
[5] V. Godbole, C. Villevieille, H. Sommer, J.-F. Colin, P. Novák, Electrochim. Acta 77 (2012) 244–249.
[6] A. El Jazouli, S. Krimi, B. Manoun, J.P. Chaminade, P. Gravereau, D. de Waal, Ann. Chim. Sci. Mat. 23 (1998) 7–10.
[7] R. Tripathi, G. Popov, B. Ellis, A. Huq, L.F. Nazar, Energy Environ. Sci. 5 (2012) 6238–6246.
[8] J. Rodriguez-Carvajal, Fullprof, Program for Rietveld Refinement, Version 3.7 (1997). LLB JRC.
[9] Z.G. Lu, M.F. Lo, C.Y. Chung, J. Phys. Chem. C 112 (2008) 7069–7078.
[10] K.C. Park, T. Hayashi, H. Tomiyasu, M. Endo, M.S. Dresselhaus, J. Mater. Chem. 15 (2005) 407–411.
[11] G.X. Wang, X.P. Shen, J. Yao, J. Park, Carbon 47 (2009) 2049–2053.
[12] M. Doeff, Y. Hu, F. McLarnon, R. Kostecki, Electrochem. Solid-State Lett. 6 (2003) A207–A209.
[13] D. Larcher, C. Masquelier, D. Bonnin, Y. Chabre, V. Masson, J.-B. Leriche, J.-M. Tarascon, J. Electrochem. Soc. 150 (2003) A133–A139.
[14] P. Poizot, S. Laruelle, S. Grugeon, L. Dupont, J. Tarascon, Ionics 6 (2000) 321–330.
[15] K. Lasri, I. Saadoune, Y. Bentaleb, D. Mikhailova, H. Ehrenberg, L. Häggström, K. Edström, Solid State Ionics 224 (2012) 15–20.
[16] S. Patoux, C. Masquelier, Chem. Mater. 14 (2002) 5057–5068.
[17] M. Dollé, S. Patoux, T.J. Richarson, J. Power Sources 144 (2005) 208–213.
[18] P. Poizot, S. Laruelle, S. Grugeon, L. Dupont, J.M. Tarascon, Nature 407 (2000) 496–499.
[19] B. Varghese, M.V. Reddy, Z. Yanwu, C.S. Lit, T.C. Hoong, G.V. Subba Rao, B.V.R. Chowdari, A. Thye, S. Wee, C.T. Lim, C.-H. Sow, Chem. Mater. 20 (2008) 3360–3367.
[20] X.H. Huang, J.P. Tu, C.Q. Zhang, F. Zhou, Electrochim. Acta 55 (2010) 8981–8985.
[21] P. Poizot, S. Laruelle, S. Grugeon, J. Tarascon, J. Electrochem. Soc. 149 (2002) A1212–A1217.